CSIRO PUBLISHING

International Journal of Wildland Fire **2020**, *29*, 820–831
https://doi.org/10.1071/WF19207

Effects of fuel characteristics on horizontal spread rate and ground surface temperatures of smouldering duff

Daniel A. Cowan[A], *Wesley G. Page*[B], *Bret W. Butler*[B] *and David L. Blunck*[A,C]

[A]School of Mechanical, Industrial, and Manufacturing Engineering, Oregon State University, Corvallis, OR 97331, USA.
[B]Rocky Mountain Research Station, US Forest Service, 5775 W Broadway Street, Missoula, MT 59808, USA.
[C]Corresponding author. Email: david.blunck@oregonstate.edu

Abstract. The slow-moving flameless burning of wildland fuels (i.e. smouldering) can be difficult to detect and challenging to extinguish. Although previous research involving the smouldering of organic fuels (e.g. cotton, cellulose, peat) has investigated the influence of various fuel characteristics (e.g. moisture content, inorganic content, bulk density) on spread rate and surface temperatures, the smouldering behaviour of other common fuels is not well understood. This study expands on previous research to better understand how fuel characteristics influence the smouldering behaviour of duff from coniferous forests. Specifically, horizontal spread rates (0.5–19.5 cm h^{-1}) and ground surface temperatures (258–392°C) were measured on 52 duff samples collected from underneath mature ponderosa pine trees (*Pinus ponderosa*) from sites in the Pacific Northwest, USA, and evaluated in terms of their moisture content (6–113%), inorganic content (3–42%), bulk density (34–130 kg m^{-3}) and fuel depth (3.8–16.3 cm). The data suggested that horizontal spread rates decrease when inorganic content, inorganic loading and/or moisture loading of the duff increases. Surface temperatures decrease when inorganic bulk density and/or fuel loading increases. Conversely, surface temperatures decrease when moisture content increases for shallow duff. Higher fuel loading increases the likelihood of smouldering below the surface.

Additional keywords: ponderosa pine, wildfire.

Received 12 December 2019, accepted 10 May 2020, published online 6 July 2020

Introduction

Smouldering combustion during wildfires has a variety of impacts on several important ecological and sociological systems (Rappold *et al.* 2011; Watts and Kobziar 2013). As compared with flaming combustion, smouldering combustion can burn in lower-oxygen environments (Huang and Rein 2016; Wang *et al.* 2017) and at lower temperatures (Anderson *et al.* 2000). These characteristics allow smouldering to propagate subsurface (Rein 2009; Huang and Rein 2019) and burn for extended periods of time (Ohlemiller 1985; Rein 2013). The heating related to the long duration of smouldering combustion can lead to plant death and soil sterilisation (Ryan and Frandsen 1991). The characteristics of smouldering can also allow wildfires to persist without detection and transition into flaming combustion, even after several months (Wein 1981; Pawlitz 2018).

Although forests make up ~33% of the United States of America's surface area (Oswalt and Smith 2014), our understanding of smouldering behaviour (e.g. spread rate, temperature) within duff is quite limited. Duff is comprised of decomposing plant litter such as needles, bark, twigs and cones. Duff naturally forms layers as the amount of decomposition in the plant litter increases with depth. The lower duff layer (i.e. Oa and humus) typically has higher mineral content and bulk density compared with the upper duff layer (i.e. Oe and fermentation) (Garlough 2010). Moisture content (MC) in the lower duff is more homogeneous than the upper duff because the upper duff is exposed to environmental conditions (Johnson *et al.* 2013). The stratification and variation in fuel characteristics (e.g. MC, inorganic content) of duff add complexity to understanding smouldering behaviour. Therefore, research on smouldering duff with respect to fuel characteristics is needed to better predict the behaviour of smouldering during prescribed burns and wildfires.

The limited studies considering smouldering combustion within duff have typically focused on identifying the impact of fuel characteristics on smouldering sustainability and fuel consumption. For example, Frandsen (1997), and later Garlough (2010), examined how MC and inorganic content (IC) affect fuel consumption, and found that MCs ranging from 90 to 150% will prevent smouldering in organic soils (e.g. duff) with low IC (0 to 10%), whereas dry fuels (MC up to 20%) will deter smouldering when IC ranges from 55 to 80% (Frandsen 1987, 1997; Garlough 2010; Huang and Rein 2015). MC and IC both act as heat sinks during smouldering (Ohlemiller 1985; Huang and Rein 2014). Garlough (2010 found that bulk density does not play a role in smouldering sustainability or duff consumption rates. What has not been considered in studies of smouldering duff is the role fuel characteristics play in influencing smouldering spread rate and temperatures.

Other studies have related fuel characteristics to observed smouldering behaviour within natural fuels (e.g. cotton, cellulose and peat). The natural fuels were prepared from isolated, clean sources that would not typically be observed in forests. It was found that increased MC decreases smouldering horizontal spread rates and surface temperatures (Prat-Guitart *et al.* 2015; Huang *et al.* 2016). For example, Huang *et al.* (2016) found that dry peat (MC of 5%) can have smouldering surface temperatures 200°C hotter and surface horizontal spread four times faster than moist fuels (MC of 100%) (Huang *et al.* 2016). Yang and Chen (2018) found that increased IC decreases smouldering vertical spread rates within peat. An additional 200% increase in IC of the peat resulted in the smouldering vertical spread rate decreasing by 50% (Yang and Chen 2018). Smucker *et al.* (2019) found that an increase in bulk density from 200 to 300 kg m^{-3} resulted in the horizontal spread rate decreasing by 40% for smouldering within cellulose. The decrease in horizontal spread rate with increased bulk density is also observed in other natural fuels (Hagen *et al.* 2011; Prat-Guitart *et al.* 2016; Smucker *et al.* 2019). These studies of smouldering behaviour within natural fuels further provide insight into the effects that MC, IC and bulk density may have within duff.

The objective of the present study was to determine the relative significance of MC, IC, organic bulk density and fuel thickness (i.e. depth) on influencing horizontal spread rate and ground surface temperatures (also referred to as surface temperatures) within smouldering duff. To satisfy this objective, surface temperatures and propagation rates were measured as ponderosa pine (*Pinus ponderosa*) duff smouldered. An ordinary least-squares regression was used to characterise the smouldering behaviour with respect to several fuel characteristics. The regression models were evaluated by applying them to results from field-scale prescribed fires. Although this study focuses on ponderosa pine duff, the layering, stratification and composition of duff are similar between coniferous tree species (Waksman 1936; Van Wagtendonk *et al.* 1998); therefore, the influence of the fuel characteristics on smouldering behaviour is expected to be similar for duff from other coniferous trees.

Experimental approach

Sample collection

The smouldering behaviour of 52 ponderosa pine duff samples was evaluated. Forty-seven tests were conducted in a laboratory and five tests were conducted in the field. The 47 laboratory samples were collected beneath mature ponderosa pine trees from Oregon (USA), and the field tests were performed in Washington and Montana (locations in Appendix A1). The laboratory samples had dimensions of 46 × 46 cm and the field samples had dimensions of 50 × 50 cm. All samples were selected within 2 m of the tree bole such that the duff depth was at least 5 cm across the entire sample area. In order to preserve each laboratory sample's physical integrity, an extraction jig was used to remove the samples from the field by utilising four sharpened sheet metal blades arranged on the four sides of the frame to isolate each sample. The sharpened sheet metal blades were hammered to a depth of roughly 20 cm. The surrounding duff was removed. An additional sheet metal blade was hammered under the jig where at least 2 cm of mineral soil base was removed. The sample was slid into a three-sided cardboard box, after which the box was formed to contain the sample. Pictures of duff samples and of samples being extracted are available (Cowan 2020). Samples were stored in their cardboard boxes within a conditioned building (approximate temperature 21°C and humidity between 30 and 50%) until the smouldering test.

Sample characterisation

Prior to ignition, each sample was prepared and fashioned to have the fuel characteristics measured. First, the litter layer (i.e. fresh pine needles, bark chips and sticks) was removed to have a better view of the duff during testing (note: discoloured, grey needles were considered part of the duff). Second, subsamples of the duff were extracted from the four corners. The upper and lower duff thickness was measured from the extracted void. The subsamples were analysed (as described later) to obtain a representative MC, IC and organic bulk density. Fig. 1 shows histogram plots of the fuel characteristics for both the upper and lower duff for the laboratory samples.

The extracted subsamples were divided by composition into the upper and lower duff layer, as illustrated in Fig. 2. The mass of each layer was measured. The upper duff layer is heterogeneous and contains organic materials that can be identified (e.g. pine bark, pinecones or pine needles). The lower duff is more homogeneous because the organic material structure is mostly decomposed (Waksman 1936).

The upper duff's fuel characteristics were used when determining the effects of fuel characteristics on smouldering behaviour. Upper duff was selected because the surface temperature would be representative of the upper duff burning, and smouldering typically spread horizontally in this layer. Bulk density was represented by the organic bulk density. Organic bulk density was selected because it represents the combustible fuel available per unit volume. The MC was determined using ASTM D2974–87 Method B (ASTM International 1993). The IC was determined from the method outlined by Nelson and Sommers (1996). Appendix A2 has a complete list of the properties of each sample that was burned.

Experimental approach

The experimental arrangement included an infrared (IR) camera with a stainless-steel mirror to reflect emitted radiation, thermocouples, a visual camera and a coflow (see Fig. 3). A stainless-steel mirror was selected because it has a relatively high reflectivity in the near-IR spectrum. The stainless-steel mirror and the coflow were not used for the field samples. The images from the IR camera (laboratory tests: FLIR SC6700; field tests: Mikron MikroScan-7200) enabled smouldering horizontal spread rates to be determined. The IR camera was also used to determine smouldering surface temperatures for laboratory tests. A thermocouple (type-K) was used to validate the temperature range obtained from the IR camera. The visual camera (laboratory tests: Canon EOS Rebel T3i; field tests: Go Pro Hero 3+) was used to visualise the burn and record when smouldering transitioned to flaming. Samples were tested within the cardboard box that they were collected and stored in. This allowed minimal disturbances to the sample. Admittedly, the thermal and mass transport properties of the cardboard are different than those of soil.

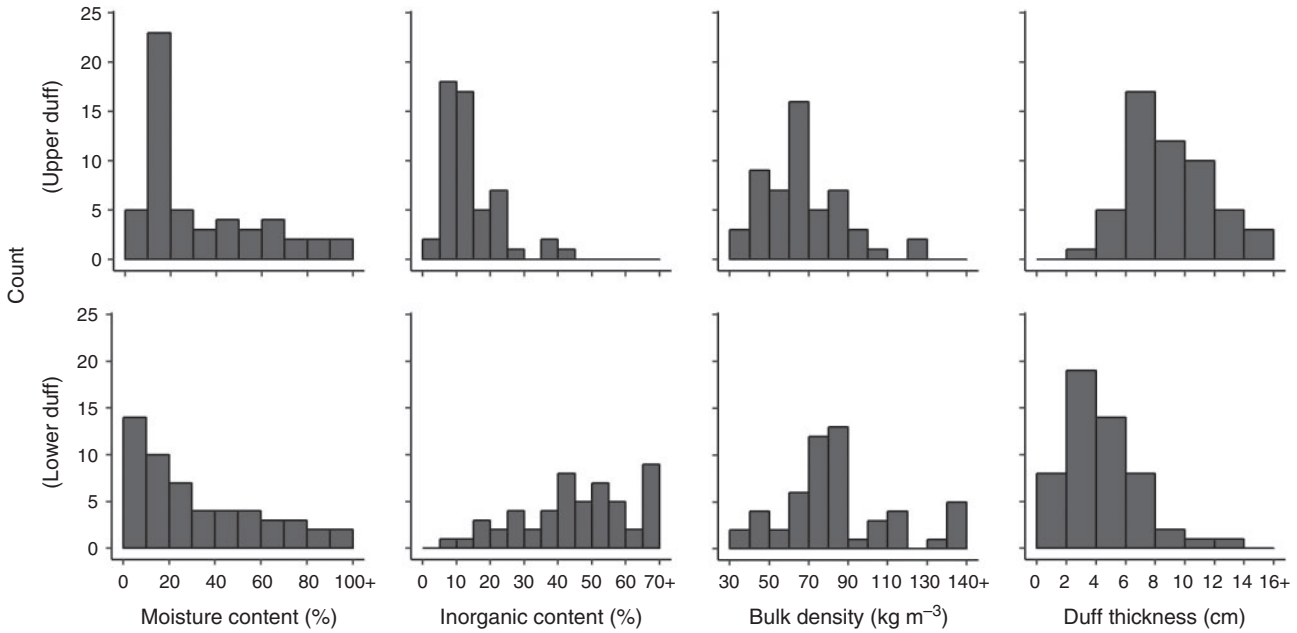

Fig. 1. Histogram plots of the measured moisture content (MC), inorganic content (IC), organic bulk density and duff thickness for the upper and lower duff.

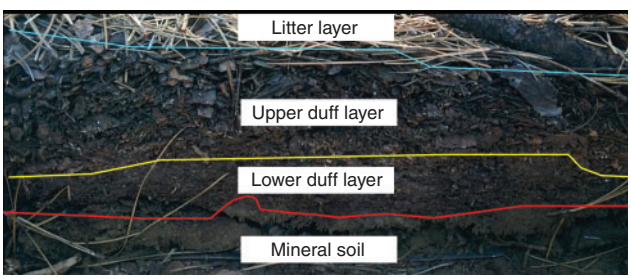

Fig. 2. Cross-section of a sample collected in the field. The upper duff contains the organic matter that is still recognisable. The lower duff layer is more homogeneous with organic matter that is highly decomposed.

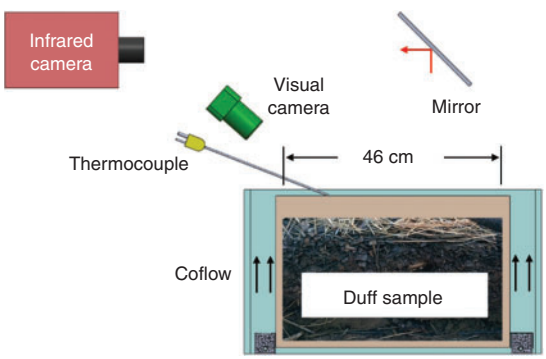

Fig. 3. Experimental arrangement for measuring horizontal spread rates and surface temperatures during smouldering combustion.

Nonetheless, the impact of these discrepancies on smouldering behaviour is expected to be minimal considering that burns occurred primarily away from the boundaries.

The coflow provided a low-velocity (<0.2 m s^{-1}) sheath of dry air (from a compressor) flowing upward around the sample during laboratory burns to reduce the variability of the relative humidity observed at the surface of the sample during cold tests (temperature <15°C). The ventilation system, operating to remove exhaust, drew in exterior air that had relative humidity as high as 98%. The coflow was turned on 15 min before the smouldering test and the temperature and humidity above the sample were recorded. The coflow controlled the relative humidity around the sample to a mean value of 51% with a standard deviation of 11%. The coflow was heated, which resulted in the mean temperature above the plot being 14°C with a standard deviation of 5°C.

The sample was ignited using a 1500-W heat gun with a diameter of 2.5 cm. The heat gun was applied at the centre of the sample with the nozzle lightly touching the duff. The heated air penetrated the upper duff to heat the lower layers. The nozzle applied heat until the sample ignited with flaming combustion. Immediately after flaming occurred, the flames were gently smothered using a leather glove. The sample was monitored for the first 2 h to ensure that smoke was present or that the IR camera was reading a photon count of at least 1300 (corresponding to 230°C). If smoke was not present and the photon counts measured by the IR camera were less than 1300, the heat gun was reapplied until flaming combustion reoccurred. The ignition process was repeated as needed until smouldering was observed or the time from initial ignition exceeded 2 h. IR image data for 5 min after ignition were not used to determine smouldering behaviour to reduce bias from ignition on the results. If the time exceeded 2 h without sustained smouldering, the sample was considered not to have smouldered. Two of the 47 laboratory and one of the field tests were considered not to have smouldered and were not included in the data analysis.

If the sample transitioned to flaming combustion during testing, the flames were gently smothered by a leather glove. The flaming incident was recorded, and the sample was allowed to continue smouldering. The smouldering behaviour (i.e. propagation rates and surface temperatures) was determined exclusive of the flaming incidents. The smouldering test was considered concluded when the smouldering front reached 5 cm from the sample perimeter. Smouldering test times ranged from 1.5 to 14 h.

The visual and IR cameras acquired images every 10 s during testing. The IR camera had an integration time of 4.96 ms. This integration time was selected to match a temperature range from 80 to 730°C, which contains smouldering combustion temperatures (Anderson *et al.* 2000; Rein 2013). Before igniting the sample, a spatial calibration image was taken with both the visual and IR cameras to be used in the data analysis. Representative visible images of smouldering duff are available (Cowan 2020).

The IR camera images indicated the smouldering location, classified as surface or subsurface. Smouldering was considered surface smouldering if fuel discoloration (indicating pyrolysis) spread as a continuum whereas subsurface smouldering had intermittent discoloration as it spread subsurface, then resurfaced at a different location. Subsurface smouldering is where the smouldering front is travelling faster below the surface and not visible (visible spectrum) until the front resurfaces. Forty-four of the 49 samples that were ignited were classified as surface smouldering. All the field studies were surface smouldering. In surface smouldering samples, the leading edge of the smouldering front was commonly observed below the topmost fuels (e.g. grey pine needles, bark chips), but the topmost fuels smouldered shortly after the edge passed. The leading edge of the smouldering front was similarly observed slightly below the surface in other studies (Frandsen 1997; Huang *et al.* 2016).

Image processing

The surface temperatures of smouldering duff were determined from the IR images collected during laboratory burns. A blackbody calibration, using an Electro Optical Industries, Inc. CS series blackbody, was performed to relate the measured photon counts to the temperature with a measurement error of 1%. An emissivity of 0.85 (standard deviation of 0.03) was applied when determining the surface temperatures of burning duff samples. The emissivity of the duff was determined based on 22 thermocouple measurements of temperatures (144 to 550°C) corresponding to their respective location within the IR images. An emissivity of 0.85 is similar to the values measured for heated wood (60°C) (López *et al.* 2013) and burning grey charcoal (Vanaparti 2016). Quantified temperature values were not obtained for the IR camera used in the field; therefore, these results were not included for statistical modelling.

The spatial calibration for the IR images was determined before ignition based on heated markers located in each of the four quadrants of the plot. To validate the calibration, the distance between two opposing corners was determined using the image and compared with the actual distance. The difference between the physical distance and the calibration was less than 5% of the physical distance.

The IR images were time-averaged every 30 s (i.e. three frames). The time-averaging was performed in order to reduce the effect of smoke blocking the view within a single image. The time-averaged images were subsequently used in determining horizontal spread rates and smouldering surface temperatures.

A temperature threshold was used to divide pixels into locations corresponding to smouldering or not, and ultimately determine the horizontal spread rate. A temperature of 110°C or higher was selected as the smouldering threshold in the IR images when determining spread rate. This threshold was selected based on observed locations where smoke was released and for being above the temperature of a non-smouldering region (no smoke). The temperature threshold was lower than temperatures of a smouldering front because the front was commonly below the surface. In these instances, the spread rate was determined based on the changes in the surface temperature just above a smouldering front. Smoke was observed leaving these regions of elevated surface temperatures, further confirming the existence of the smouldering front.

A smouldering region and its perimeter were located from the pixel temperatures (examples shown in Fig. 4*a*, *b*), and were classified as smouldering in subsequent images. This approach reduced the effects of temperature fluctuations (cooling and reheating) on the measured horizontal spread rate.

The horizontal spread rate was determined by measuring the differences in the location of the perimeter at 10-min increments. Equally spaced points (0.5 cm) around the outter perimeter determined the number of velocity vectors found. The shortest distance between each point and the previous perimeter was used to determine the horizontal spread velocity. The spread velocities were calculated around the perimeter of the smouldering region and throughout time. This approach allowed variation (both spatially and temporally) in horizontal spread rate to be determined (example shown in the right panel of Fig. 4). The horizontal spread rate of the sample was determined by averaging all the measured horizontal spread velocities (both spatially and temporally). Image processing was managed using *Python 2.7* and *OpenCV*.

The mean smouldering surface temperature for the burn was obtained by averaging all pixel locations in all the images that had a temperature greater than 250°C. The threshold of 250°C was chosen because natural fuel pyrolysis starts to occur near this temperature (Zhao *et al.* 2014). The mean smouldering surface temperature does not include elevated surface temperatures caused by subsurface smouldering regions.

Data analysis

Statistical models were created for identifying the fuel characteristics that influenced smouldering subsurface probability, horizontal spread rate and surface temperature. The measurements from 45 laboratory tests were considered. The explanatory variables considered were MC, IC, organic bulk density, duff thickness and an indicator variable for subsurface smouldering for the horizontal spread rate and surface temperature models. Automated model selection for all possible combinations of the explanatory variables was performed using the package glmulti (Calcagno and de Mazancourt 2010) in *R* (version 3.5.1) by selecting the model with the smallest Akaike information criterion (AIC) (Akaike 1974).

The model for subsurface smouldering probability was selected by comparing factorial logistic models. All possible

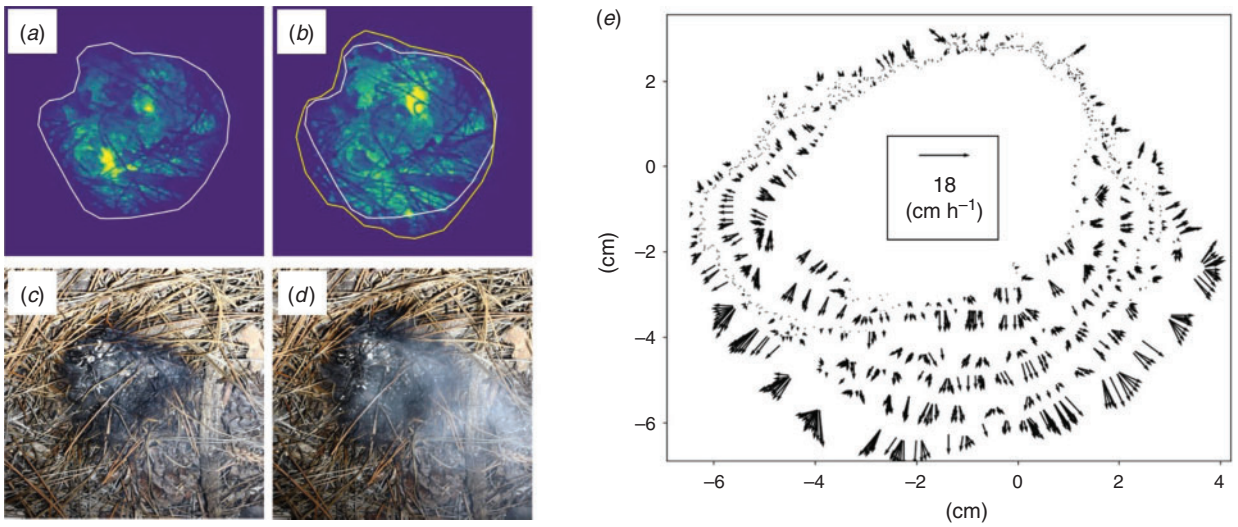

Fig. 4. (*a*) IR image of smouldering duff with the corresponding smouldering perimeter outlined. (*b*) IR image 10 min after (*a*) with new perimeter. Brighter colours correspond to hotter temperatures. Panels (*c*) and (*d*) are visual images corresponding respectively to (*a*) and (*b*). Panel (*e*) is a quiver plot showing the horizontal spread rates as they appear within a close-up of the smouldering sample. A ring of arrows pointing outwards corresponds to the horizontal spread rate determined at 10-min intervals.

reduced factorial logistic regression models were compared from the full factorial logistic regression model. All the fuel characteristics and fuel characteristic interactions are considered in the full model as:

$$P_I = \frac{1}{1+\exp\left[-\left(\beta_0 + \sum_{i=0}^{3}(\beta_{+1}C_i) + \sum_{j=0}^{2}\left(\sum_{k=j+1}^{3}(\beta_{+1}C_jC_k)\right)\right)\right]} \quad (1)$$

where P_I is the probability that the burn is subsurface and C_0, C_1, C_2, and C_3 respectively represent MC, IC, organic bulk density and duff thickness from the upper duff. The β terms are the coefficients for the fuel characteristics. The subscript '+1' implies that a new coefficient is needed for each addition of a respective variable or interaction.

A natural log-transformation of horizontal spread rate was performed before model selection. The log-transformation was performed in order to meet the assumptions to perform a linear regression model. The model selected for the natural log-transformation of spread rate examined all possible reduced linear models of the full model:

$$log(S) = \beta_0 + \sum_{i=0}^{4}(\beta_{+1}C_i) + \sum_{j=0}^{3}\left(\sum_{k=j+1}^{4}(\beta_{+1}C_jC_k)\right) \quad (2)$$

where S is the horizontal spread rate and C_4 represents an indicator variable for when the smouldering location was subsurface. The β terms are the coefficients of the explanatory variables and their interactions. The subscript '+1' for β represents a new coefficient for the respective variable or interaction. The β terms are coefficients estimated from the data. Only the laboratory tests were included when selecting a model and determining estimates for β.

Model selection for the surface temperature examined all possible reduced linear models of the full model:

$$T_s - T_\infty = \beta_0 + \sum_{i=0}^{4}(\beta_{+1}C_i) + \sum_{j=0}^{3}\left(\sum_{k=j+1}^{4}(\beta_{+1}C_jC_k)\right) \quad (3)$$

where T_s is the smouldering surface temperature. The left side of the equation allows the mean increase in temperature caused by smouldering to be compared with the fuel characteristics and fuel characteristics' interactions.

In order to evaluate the performance of the models, they were applied to the values obtained from four field tests. The mean absolute percentage error (MAPE), root-mean-square error (RMSE), mean bias error (MBE), mean absolute error (MAE) and whether the model predictions were within the 95% prediction intervals are reported for spread rate (Cruz and Alexander 2013). Note that the smouldering surface temperature model was not compared with the field tests because the IR camera for the field tests was not calibrated for temperature.

Results and discussion

The average horizontal spread rates ranged from 0.5 to 3.1 cm h^{-1} (mean 2.1 cm h^{-1}) for subsurface burns and from 0.7 to 19.5 cm h^{-1} (mean 7.2 cm h^{-1}) for surface burns. The faster speeds for the latter are attributed to greater oxygen availability at the smouldering location. Fig. 5 shows a box-and-whisker plot for both spread rates and surface temperatures. The average smouldering surface temperatures for each test ranged from 260 to 310°C (mean 280°C) for subsurface burns and from 280 to 390°C (mean 320°C) for surface burns. These propagation rates and temperatures are consistent with those reported for peat. Huang *et al.* (2016) found horizontal spread rates within peat (without wind

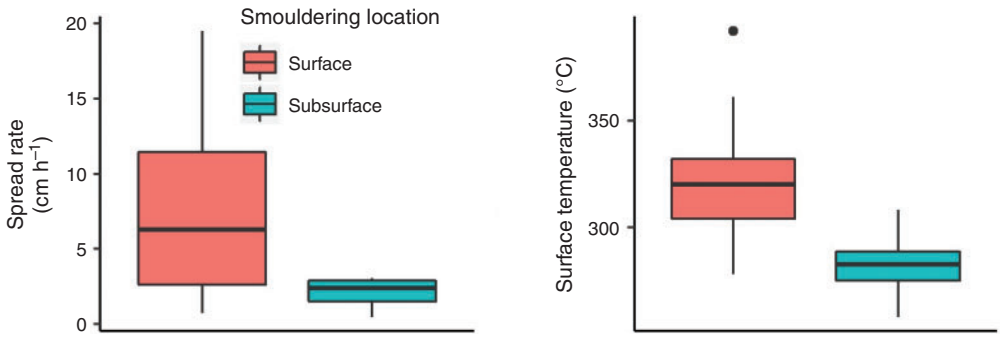

Fig. 5. Box-and-whisker plot of smouldering spread rate (left panel), and surface temperatures (right panel) for surface and subsurface smouldering.

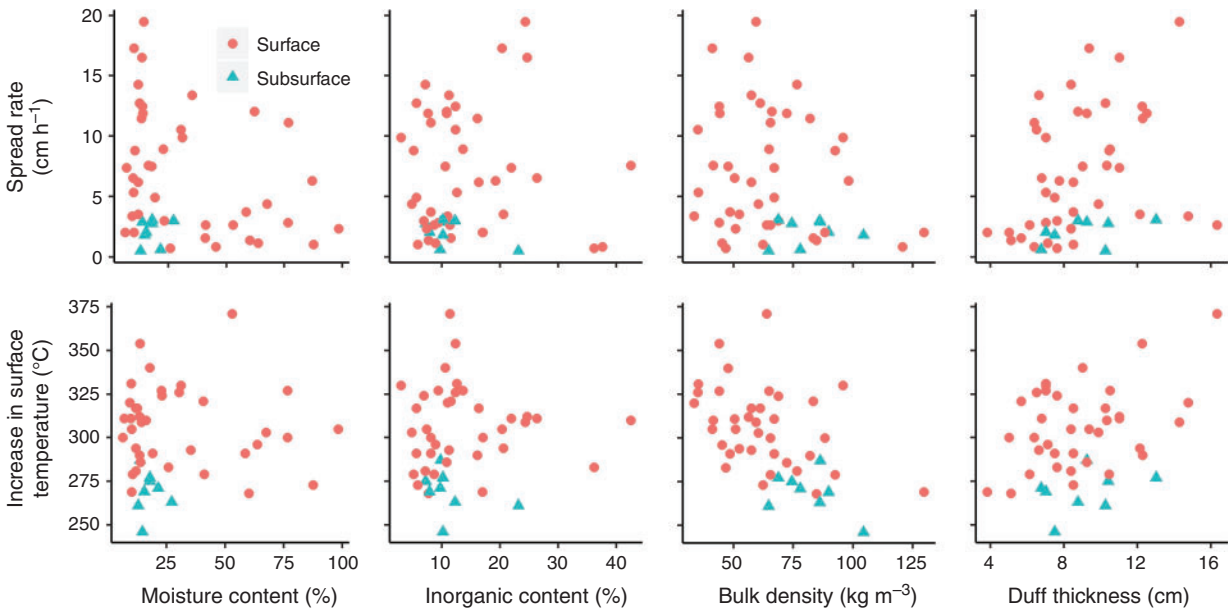

Fig. 6. Scatter plots showing horizontal spread rate and increase in smouldering surface temperatures from ambient with respect to moisture content (MC), inorganic content (IC), organic bulk density and duff thickness for the upper duff. The red and blue symbols represent surface and subsurface smouldering respectively.

assistance) ranged from 2 to 12 cm h^{-1} depending on MC, and that surface temperatures ranged from under 200 to over 500°C (Huang *et al.* 2016).

Fig. 6 shows the horizontal spread rates and surface temperatures plotted with respect to MC, IC, organic bulk density and duff thickness for the upper duff. The figure displays the range of smouldering behaviour with respect to the fuel characteristics included in the analysis. Both spread rate and surface temperature are noticeably lower for subsurface smouldering, as expected. The relatively large range in the smouldering behaviour for each fuel characteristic suggests that smouldering behaviour cannot be explained by a single fuel characteristic.

Statistical analysis was applied to better understand the influence of the physical conditions of the fuel on the smouldering behaviour. The resulting reduced statistical models (from respective full models Eqns 1, 2 and 3) for probability of subsurface smouldering (P_I), horizontal spread rate (S, cm h^{-1}) and smouldering surface temperature (T_s, °C) are respectively shown as:

$$P_I = \frac{1}{1 + exp(-(\beta_0 + \beta_1 Z + \beta_2 \mathrm{MC} \cdot \mathrm{IC} + \beta_3 \rho \cdot Z))} \quad (4)$$

$$log(S) = \beta_0 + \beta_1 \mathrm{IC} + \beta_2 \mathrm{MC} \cdot Z + \beta_3 \mathrm{IC} \cdot Z + \beta_4 \mathrm{IC} \cdot I \quad (5)$$

$$T_s = T_\infty + \beta_0 + \beta_1 \mathrm{MC} + \beta_2 I + \beta_3 \mathrm{MC} \cdot Z + \beta_4 \mathrm{IC} \cdot \rho + \beta_5 \rho \cdot Z \quad (6)$$

Here, T_∞ is the ambient temperature (°C), MC (%) is from the upper duff, IC (%) is from the upper duff, ρ (kg m^{-3}) is the organic bulk density from the upper duff, Z (cm) is the thickness of the upper duff, and I represents an indicator variable for subsurface smouldering location. The estimates for the β terms and their significance are shown in Table 1.

Table 1. The estimated coefficients ($\hat{\beta}$) for Eqns 4 (subsurface probability), 5 (spread rate), and 6 (surface temperature)

The *P* value significance is given to the right of the estimated coefficients where $0.1 > ^{x} \geq 0.05 > * \geq 0.01 > ** \geq 0.001 > ***$. Here, moisture content (MC) (%) is from the upper duff, inorganic content (IC) (%) is from the upper duff, ρ (kg m^{-3}) is the organic bulk density from the upper duff, Z (cm) is the thickness of the upper duff, and I represents an indicator variable for when the smouldering location was subsurface

	Subsurface probability Eqn 4			Log spread rate Eqn 5			Surface temperature Eqn 6		
$\widehat{\beta}_0$	(Intercept)	−3.18		(Intercept)	2.51	***	(Intercept)	347	***
$\widehat{\beta}_1$	(Z)	−0.465	x	(IC)	−0.112	***	(MC)	−1.63	***
$\widehat{\beta}_2$	(MC · IC)	−0.0013		(MC · Z)	−0.002	***	(I)	−32.8	***
$\widehat{\beta}_3$	($\rho \cdot Z$)	0.0097	*	(IC · Z)	0.010	***	(MC · Z)	0.173	***
$\widehat{\beta}_4$				(IC · I)	−0.112	***	(IC · ρ)	−0.0147	*
$\widehat{\beta}_5$							($\rho \cdot Z$)	−0.0433	*
R^2_P		0.28	**		0.51	***		0.53	***

Table 2. The field measurements compared with the model fits

Location	Observed smouldering location	Predicted subsurface probability	Measured spread rate (cm h^{-1})	Predicted spread rate (95% prediction interval)		
				Fit	Lower bound	Upper bound
Winthrop, WA (1)	Surface	7.8%	12.06	2.96	0.73	12.07
Winthrop, WA (2)	Surface	30.9%	0.84	1.04	0.20	5.40
Winthrop, WA (3)	Surface	18.7%	6.30	1.51	0.34	6.66
Missoula, MT	Surface	12.8%	1.38	4.02	1.01	16.04

It is important to note that the R^2_p values are relatively low (see Table 1), which effectively means that the fitted equations should not be used for predicting smouldering behaviour; however, the relationships derived can still be of significance. Furthermore, if the R^2_p value is low, but coefficients are significant (P value < 0.05), important conclusions on how fuel characteristics impact smouldering behaviour can still be drawn. Regardless of the R^2_p, the significant coefficients still represent the mean change in the response for one unit of change in the predictor while holding other predictors in the model constant. This type of information can be extremely valuable in understanding what controls smouldering behaviour.

The interaction between organic bulk density and duff thickness ($\widehat{\beta}_3$) is the only statistically significant (P value <0.05) term in the subsurface probability equation. The other terms ($\widehat{\beta}_1$ and $\widehat{\beta}_2$) allow for a more accurate model, but there is inconclusive evidence that duff depth or the interaction between MC and IC affect subsurface smouldering. This interaction represents the organic fuel loading (mass of fuel per area). If there is more fuel, there is a higher probability that the smouldering front will travel subsurface. As more fuel covers the ground, there is more subsurface fuel. It is likely that the additional fuel below the surface increases subsurface smouldering probability.

The subsurface probability equation,

$$P_1 = \frac{1}{1 + exp(-(-3.18 + -0.464 \cdot Z + -0.0013 \cdot MC \cdot IC + 0.0097 \cdot \rho \cdot Z))} \quad (7)$$

was applied to the fuel characteristics from the field-based tests (Table 2) to evaluate the applicability of the results from the laboratory burns to the field. The highest predicted subsurface probability was 30.9%. Three of the burns had a less than 20% probability of subsurface burning. During the actual burns, all of smouldering was observed at the surface, consistent with the predictions.

The fitted median horizontal spread rate derived from statistical model Eqn 5 is:

$$log(S_{surface}) = 2.51 - 0.112\text{IC} - 0.002\text{MC} \cdot Z - 0.015\text{IC} \cdot Z \quad (8a)$$

$$log(S_{subsurface}) = 2.51 - 0.224\text{IC} - 0.002\text{MC} \cdot Z - 0.015\text{IC} \cdot Z \quad (8b)$$

for both surface ($S_{surface}$) and subsurface ($S_{subsurface}$) smouldering respectively. Note that the relationships are correlated with IC, moisture loading (MC · Z) and the inorganic loading (IC · Z) for the upper duff. All three terms have statistical evidence (P value <0.001) that they affect spread rate.

Increasing IC decreases spread rate (P value <0.001). Yang and Chen (2018) reported that increasing IC can decrease the downward spread rate in peat by limiting the heat transfer between two adjacent fuel particles and limiting oxygen diffusion (Yang and Chen 2018). The IC should have a similar role within the duff. This is further displayed in the subsurface spread rate equation, which has IC affecting the log spread rate twice as much as surface spread rate (−0.112 *v.* –0.224).

Similarly, increasing inorganic loading (IC · Z) decreases the spread rate (P value <0.001). The inorganic loading represents the mass of inorganic content within the duff per area. As smouldering occurs, duff with a higher inorganic loading will

form a larger ash layer on top. The larger ash layer would further reduce oxygen diffusion into the duff, thus slowing spread rate. The relative importance of both IC and inorganic loading on spread rate has over twice the impact of moisture loading.

Increasing moisture loading ($MC \cdot Z$) also decreases spread rate. The moisture loading represents the mass of water within the duff per area. Peat smouldering studies found that MC acts as a heat sink, which slows spread rate (Huang *et al.* 2016; Prat-Guitart *et al.* 2016). The moisture loading in the duff would play a similar role to a heat sink, but also includes a depth component. This depth component is needed to account for vapour particle diffusion out of the duff. If the duff is thicker, the water vapour cannot leave the duff as readily. The vapour is more likely to condense on surrounding unburnt fuels.

By applying the spread rate model (Eqn 8) to the field smouldering test fuel characteristics, the model fit and 95% prediction interval were obtained (Table 2). The MAPE, RMSE, MBE and MAE were found using the fit and measured spread rates, and were 92%, 5.21 cm h^{-1}, 2.76 cm h^{-1} and 4.18 cm h^{-1} respectively. This indicates that the model fit does not predict the measured values accurately, which was expected based on the model's R^2_p being 0.51. Although the fit ranges from being 4.07 times too small to 2.91 times too large, the model's 95% prediction interval bounds the measured spread rate, which indicates that the model is capturing some of the physics that control smouldering of duff.

The fitted mean surface temperature derived from model Eqn 6 is:

$$T_{s,surface} = T_\infty + 347 - 1.6MC + 0.17MC \cdot Z - 0.015IC \cdot \rho - 0.043\rho \cdot Z \quad (9a)$$

$$T_{s,subsurface} = T_\infty + 314 - 1.6MC + 0.17MC \cdot Z - 0.015IC \cdot \rho - 0.043\rho \cdot Z \quad (9b)$$

for surface ($T_{s,surface}$) and subsurface smouldering tests ($T_{s,subsurface}$) respectively. The temperatures are correlated with MC, the interaction between MC and duff thickness (Z), the interaction between IC and organic bulk density (ρ), and the interaction between organic bulk density and duff thickness for the upper duff. All the fitted correlated coefficients are statistically significant (P value <0.05). The temperature model was not applied to the results from the field tests because the camera was not calibrated. It was noted that the surface temperature for subsurface smouldering was lower than the actual temperature of the smouldering front.

Increasing the MC decreases surface temperatures for plots with smaller duff thicknesses (i.e. <9 cm). Decreasing temperatures with increased MC are attributed to heat losses associated with evaporating moisture. This finding is supported by peat smouldering studies where the MC acts as a heat sink, reducing the smouldering temperature in peat (Huang *et al.* 2016; Prat-Guitart *et al.* 2016).

In contrast, increasing the MC leads to higher surface temperatures as the duff thickness is greater than 9 cm. The MC–duff thickness interaction effect is attributed to moisture stratification within the duff. When samples were stored, the duff dried because of the room's relatively low humidity (i.e. 30 to 50%). Allowing organic soils to dry in ambient air results in MC being lowest near the surface and increasing with depth (Benscoter *et al.* 2011). When the upper duff layer was thick (>9 cm), the MC near the surface (near where burning occurred) was not representative of the average MC in the upper duff. The lower MC would result in less heat loss (at the surface) and higher temperatures. It is expected that this interaction term can be present in the field when weather conditions cause duff to dry and illustrates the need to consider both local and average fuel characteristics when evaluating anticipated smouldering behaviour.

Increasing the IC and organic bulk density interaction term tends to decrease the mean smouldering surface temperature. The IC–organic bulk density interaction effectively represents the inorganic bulk density because of the relatively low IC in the duff. To show that the IC–organic bulk density can represent the inorganic bulk density, the model was refitted with the inorganic bulk density replacing the IC–organic bulk density interaction term, which resulted in no changes to the estimates' sign or their respective significance. Increasing inorganic bulk density decreases oxygen diffusion into peat (Yang and Chen 2018). The slower oxygen diffusion limits reaction rates and lowers the heat generation rate.

Increasing the organic bulk density and duff thickness interaction term decreases the mean smouldering surface temperature. The organic bulk density–duff thickness effectively is the organic fuel loading (mass of fuel per surface area). The sensitivity of the surface temperature to the fuel loading is attributed to influences of smouldering location, ignition process and burn duration. Higher fuel loading increases the amount of fuel that is subsurface, which in turns allows smouldering to burn in fuel layers below the surface. During ignition, a chimney is often formed at the heat gun location because the heated air travels down into the porous duff and burns a crater. The chimney may allow more ready transport of air and hot gases and is believed to allow more hot gases to escape instead of heating the top-most fuel. The lead smouldering front would be travelling below the surface underneath fuel that is not smouldering. Because the burn was extinguished before the top-most fuel smouldered, the surface temperatures are artificially lower than if the top-most fuel smouldered.

Summary and conclusions

Horizontal spread rates (0.5–19.5 cm h^{-1}) and ground surface temperatures (258–392°C) were measured for smouldering ponderosa pine duff in laboratory and field tests. The location of the smouldering (i.e. surface or subsurface) was noted for the different burns. The MC (6–113%), IC (3–42%), bulk density (34–130 kg m^{-3}) and fuel depth (3.8–16.3 cm) were measured and correlated with the smouldering behaviour to provide physical insights into influences on burning behaviour. Statistical models were created for subsurface smouldering probability, spread rate and surface temperature from laboratory smouldering tests. The subsurface smouldering probability model and spread rate model were compared with field smouldering tests, but failed to predict the spread rate. The model's 95% predicted spread rates bounded the measured spread rates, which implies that some of the smouldering physics is captured

in these models. The specific conclusions from this work are as follows for the range of conditions evaluated:

(1) Subsurface smouldering is more likely as fuel loading ($\rho \cdot Z$) increases.
(2) Smouldering spread rates decrease as IC increases, inorganic loading ($IC \cdot Z$) increases, and moisture loading ($MC \cdot Z$) increases. The influence of IC doubles if smouldering occurs subsurface. Horizontal smouldering propagation rates are the same order as those reported for peat, but peak propagation rates are faster than peat.
(3) Smouldering surface temperatures tend to decrease as MC, inorganic bulk density and fuel loading increase, but increase as the product of MC and duff thickness increases. This study found that surface temperature increases as the MC and duff thickness interaction term decreases. The sensitivity to the MC and duff thickness interaction is attributed to moisture stratification in thicker duff layers caused by the duff drying.

Although the results from this study are specific to ponderosa pine, they are expected to be representative of the smouldering characteristics and sensitivities for duff from other coniferous trees. Future testing is needed to verify this assumption.

Conflict of interest

The authors declare no conflicts of interest.

Acknowledgments

This research was funded by the Strategic Environmental Research and Development Program (SERDP) under contract no. W912HQ-16-C-0045. The collaboration with Jim Reardon at the US Forest Service is gratefully acknowledged. The laboratory assistants Ryan Diltz, Rijen Shonka and Thomas Wood are gratefully acknowledged for their assistance in setting up and performing experiments. Dr Jeff Hatten at the Forest Soils Laboratory (Oregon State University) is gratefully acknowledged for his soil expertise and sharing of equipment. We acknowledge Matt Ellis from the Methow Valley Ranger District of the Okanogan–Wenatchee National Forest, and the Montana Forest & Conservation Experiment Station (Lubrecht Research Forest) at the University of Montana for allowing smouldering field tests to be performed. The Sisters Rangers District (contact – Stephen Bishop) of the Deschutes National Forest and The Nature Conservancy of Oregon (site: Sycan March) are also acknowledged for providing duff sample collection sites.

References

ASTM International (1993) A5TM D 2974–87 Standard test methods for moisture, ash, and organic matter of peat and other organic soils. (ASTM International: West Conshohocken, PA) Available at http://www.astm.org/cgi-bin/resolver.cgi?D2974-20e1 [verified 25 May 2020].

Akaike H (1974) A new look at the statistical model identification. *IEEE Transactions on Automatic Control* **19**, 716–723. doi:10.1109/TAC.1974.1100705

Anderson MK, Sleight RT, Torero JL (2000) Ignition signatures of a downward smolder reaction. *Experimental Thermal and Fluid Science* **21**, 33–40. doi:10.1016/S0894-1777(99)00051-5

Benscoter BW, Thompson DK, Waddington JM, Flannigan MD, Wotton BM, De Groot WJ, Turetsky MR (2011) Interactive effects of vegetation, soil moisture and bulk density on depth of burning of thick organic soils. *International Journal of Wildland Fire* **20**, 418–429. doi:10.1071/WF08183

Calcagno V, de Mazancourt C (2010) glmulti: an R package for easy automated model selection with (generalized) linear models. *Journal of Statistical Software* **34**(12), 1–29. doi:10.18637/JSS.V034.I12

Cowan D (2020) Ponderosa pine smoldering study at Oregon State University. Zenodo. Available at https://doi.org/10.5281/ZENODO.3758298 [verified 25 May 2020]

Cruz MG, Alexander ME (2013) Uncertainty associated with model predictions of surface and crown fire rates of spread. *Environmental Modelling & Software* **47**, 16–28. doi:10.1016/J.ENVSOFT.2013.04.004

Frandsen WH (1987) The influence of moisture and mineral soil on the combustion limits of smoldering forest duff. *Canadian Journal of Forest Research* **17**, 1540–1544. doi:10.1139/X87-236

Frandsen WH (1997) Ignition probability of organic soils. *Canadian Journal of Forest Research* **27**, 1471–1477. doi:10.1139/X97-106

Garlough EC (2010) Factors that influence ponderosa pine duff mound consumption. PhD thesis, University of Montana, Missoula, MT, USA. Graduate Student Theses, Dissertations and Professional Papers. 429. Available at https://scholarworks.umt.edu/etd/429 [verified 25 May 2020].

Hagen BC, Frette V, Kleppe G, Arntzen BJ (2011) Onset of smoldering in cotton: effects of density. *Fire Safety Journal* **46**, 73–80. doi:10.1016/J.FIRESAF.2010.09.001

Huang X, Rein G (2014) Smouldering combustion of peat in wildfires: inverse modelling of the drying and the thermal and oxidative decomposition kinetics. *Combustion and Flame* **161**, 1633–1644. doi:10.1016/J.COMBUSTFLAME.2013.12.013

Huang X, Rein G (2015) Computational study of critical moisture and depth of burn in peat fires. *International Journal of Wildland Fire* **24**, 798–808. doi:10.1071/WF14178

Huang X, Rein G (2016) Interactions of Earth's atmospheric oxygen and fuel moisture in smouldering wildfires. *The Science of the Total Environment* **572**, 1440–1446. doi:10.1016/J.SCITOTENV.2016.02.201

Huang X, Rein G (2019) Upward-and-downward spread of smoldering peat fire. *Proceedings of the Combustion Institute* **37**, 4025–4033. doi:10.1016/J.PROCI.2018.05.125

Huang X, Restuccia F, Gramola M, Rein G (2016) Experimental study of the formation and collapse of an overhang in the lateral spread of smouldering peat fires. *Combustion and Flame* **168**, 393–402. doi:10.1016/J.COMBUSTFLAME.2016.01.017

Johnson EA, Keith DM, Martin YE (2013) Comparing measured duff moisture with a water budget model and the duff and drought codes of the Canadian Fire Weather Index. *Forest Science* **59**, 78–92. doi:10.5849/FORSCI.11-037

López G, Basterra LA, Acuña L, Casado M (2013) Determination of the emissivity of wood for inspection by infrared thermography. *Journal of Nondestructive Evaluation* **32**, 172–176. doi:10.1007/S10921-013-0170-3

Nelson DW, Sommers LE (1996) Total carbon, organic carbon, and organic matter. In 'Methods of soil analysis. Part 3. Chemical methods', Soil Science Society of America Book Series no. 5. (Eds DL Sparks, AL Page, PA Helmke, R Loeppert) Ch. 34, pp. 961–1010. (Soil Science Society of America, American Society of Agronomy: Madison, WI, USA). doi:10.2136/SSSABOOKSER5.3.C34

Ohlemiller T (1985) Modeling of smoldering combustion propagation. *Progress in Energy and Combustion Science* **11**, 277–310. doi:10.1016/0360-1285(85)90004-8

Oswalt SN, Smith WB (2014) U.S. Forest resource facts and historical trends. August, DOI: FS-1035. USDA Forest Service.

Pawlitz R (2018) Forest Service firefighters respond to Eagle Creek hotspot. USDA Forest Service.

Prat-Guitart N, Belcher C, Hadden R, Rein G, Yearsley J (2015) A laboratory study of the effect of moisture content on the spread of smouldering in peat fires. *Flamma* **6**, 35–38.

Prat-Guitart N, Rein G, Hadden RM, Belcher CM, Yearsley JM (2016) Propagation probability and spread rates of self-sustained smouldering fires under controlled moisture content and bulk density conditions. *International Journal of Wildland Fire* **25**, 456–465. doi:10.1071/WF15103

Rappold AG, Stone SL, Cascio WE, Neas LM, Kilaru VJ, Carraway MS, Szykman JJ, Ising A, Cleve WE, Meredith JT, Vaughan-Batten H, Deyneka L, Devlin RB (2011) Peat bog wildfire smoke exposure in rural North Carolina is associated with cardiopulmonary emergency department visits assessed through syndromic surveillance. *Environmental Health Perspectives* **119**, 1415–1420. doi:10.1289/EHP.1003206

Rein G (2009) Smouldering combustion phenomena in science and technology. *International Review of Chemical Engineering* **1**, 3–18.

Rein G (2013) Smouldering fires and natural fuels. In 'Fire phenomena and the Earth system: an interdisciplinary guide to fire science'. (Ed CM Belcher) pp. 15–33. (John Wiley & Sons). doi:10.1002/9781118529539.CH2

Ryan KC, Frandsen WH (1991) Basal injury from smoldering fires in mature *Pinus ponderosa* Laws. *International Journal of Wildland Fire* **1**, 107–118. doi:10.1071/WF9910107

Smucker BD, Mulky TC, Cowan DA, Kyle E (2019) Effects of fuel content and density on the smoldering characteristics of cellulose and hemicellulose. *Proceedings of the Combustion Institute* **37**, 4107–4116. doi:10.1016/J.PROCI.2018.07.047

Vanaparti A (2016) Experimental study of radiative properties of charcoal combustion in grills. PhD thesis, Auburn University, Auburn, AL, USA. Available at http://hdl.handle.net/10415/5013 [verified 25 May 2020]

Van Wagtendonk JW, Van Benedict JM, Sydoriak WM (1998) Fuelbed characteristics of Sierra Nevada conifers. *Western Journal of Applied Forestry* **13**, 73–84. doi:10.1093/WJAF/13.3.73

Waksman SA (1936) Humus origin, chemical composition, and importance in nature. *Soil Science* **41**, 395–493. doi:10.1097/00010694-193605000-00010

Wang H, Van Eyk PJ, Medwell PR, Birzer CH, Tian ZF, Possell M (2017) Effects of oxygen concentration on radiation-aided and self-sustained smoldering combustion of radiata pine. *Energy & Fuels* **31**, 8619–8630. doi:10.1021/ACS.ENERGYFUELS.7B00646

Watts AC, Kobziar LN (2013) Smoldering combustion and ground fires: ecological effects and multiscale significance. *Fire Ecology* **9**, 124–132. doi:10.4996/FIREECOLOGY.0901124

Wein RW (1981) Characteristics and suppression of fires in organic terrain in Australia. *Australian Forestry* **44**, 162–169. doi:10.1080/00049158.1981.10674309

Yang J, Chen H (2018) Natural downward smouldering of peat: effects of inorganic content and piled bed height. *Fire Technology* **54**, 1219–1247. doi:10.1007/S10694-018-0737-8

Zhao W, Chen H, Liu N, Zhou J (2014) Thermogravimetric analysis of peat decomposition under different oxygen concentrations. *Journal of Thermal Analysis and Calorimetry* **117**, 489–497. doi:10.1007/S10973-014-3696-4

Appendix A1. Sample collection information

Samples from Sisters were collected from multiple regions within the Sisters Ranger District. Samples were collected within 0.8 km from the latitude–longitude coordinate

Location		Test Type	Sample Quantity	Latitude	Longitude
Ashland, OR		Laboratory	1	42.0878	−122.5925
Missoula, MT		Field	3	46.9010	−113.4694
Silver Lake, OR		Laboratory	2	42.8670	−121.1366
Sisters, OR	Region 1	Laboratory	27	44.2936	−121.5868
Sisters, OR	Region 2	Laboratory	4	44.2871	−121.6066
Sisters, OR	Region 3	Laboratory	3	44.2934	−121.6291
Sisters, OR	Region 4	Laboratory	10	44.3163	−121.5751
Winthrop, WA		Field	2	48.6479	−120.2379

Appendix A2. Duff sample fuel characteristics for both upper and lower duff as well as the smouldering behaviour during the sample smouldering test

Test ID	Type	Location	Duff thickness (cm)		Duff bulk density (kg m^{-3})		Duff MC (%)		Duff IC (%)		Smouldering Location	Spread Rate (cm h^{-1})	Increase in surface temperature (°C)
			Upper	Lower	Upper	Lower	Upper	Lower	Upper	Lower			
1	Field	Winthrop	8.8	2.6	66	114	62	52	11	54	Surface	12.1	Not available
2	Field	Winthrop	6.4	8.3	121	108	46	52	38	50	Surface	0.8	Not available
3	Field	Winthrop	7.8	6.3	98	85	87	74	19	51	Surface	6.3	Not available
4	Laboratory	Sisters_1	10.4	4.9	74	100	18	13	7	43	Subsurface	2.8	275
5	Laboratory	Sisters_1	10.5	6.6	92	113	11	13	5	28	Surface	8.8	279
6	Laboratory	Sisters_1	9.3	5.8	86	68	14	14	10	47	Subsurface	2.9	287
7	Laboratory	Silver Lake	12.3	3.3	82	73	14	23	16	56	Surface	11.5	290
8	Laboratory	Silver Lake	14.3	0.4	59	157	14	20	24	51	Surface	19.5	309
9	Laboratory	Sisters_1	16.3	2.9	64	87	53	31	11	39	Surface	2.6	371
10	Laboratory	Sisters_2	7.6	3.3	47	16	26	28	36	80	Surface	0.7	283
11	Laboratory	Sisters_2	11.3	4	71	82	49	39	14	52		Did not smoulder	
12	Laboratory	Sisters_2	6.8	5.6	51	81	10	5	26	75	Surface	6.5	311
13	Laboratory	Sisters_2	6.5	6	35	33	30	2	12	59	Surface	10.6	326
14	Laboratory	Sisters_3	7	8.8	44	57	77	73	9	40	Surface	2.8	327
15	Laboratory	Sisters_3	7	12.3	96	81	31	60	3	12	Surface	9.9	330
16	Laboratory	Sisters_3	7.5	10.5	67	50	19	45	6	16	Surface	4.9	291
17	Field	Missoula	4.5	5.1	65	86	113	119	12	27		Did not smoulder	
18	Field	Missoula	5.1	4.5	85	117	60	105	8	23	Surface	1.4	N/A
19	Laboratory	Sisters_1	14.8	2.8	34	260	9	13	11	56	Surface	3.4	320
20	Laboratory	Sisters_1	12.5	4.5	44	50	14	13	8	44	Surface	11.9	314
21	Laboratory	Sisters_1	9	4.5	48	62	18	14	11	53	Surface	7.5	340
22	Laboratory	Ashland	7	3.8	35	73	10	9	13	44	Surface	5.3	331
23	Laboratory	Sisters_1	10.3	2.7	41	60	16	9	42	85	Surface	7.6	310
24	Laboratory	Sisters_1	11	1.8	67	88	7	5	22	73	Surface	7.4	311
25	Laboratory	Sisters_1	12.3	3.5	44	87	14	7	12	74	Surface	12.5	354
26	Laboratory	Sisters_1	12.1	4.5	52	62	12	6	21	77	Surface	3.5	294
27	Laboratory	Sisters_1	10.3	3.8	65	66	13	10	23	44	Subsurface	0.5	261
28	Laboratory	Sisters_1	11	0.5	56	114	14	23	25	79	Surface	16.5	312
29	Laboratory	Sisters_1	10.3	5.8	61	82	13	0	6	49	Surface	12.7	317
30	Laboratory	Sisters_1	9.4	0.3	41	212	10	83	20	60	Surface	17.3	305
31	Laboratory	Sisters_1	8.5	3	57	83	12	9	16	56	Surface	6.2	317
32	Laboratory	Sisters_1	5.7	3	83	72	41	22	12	39	Surface	1.6	321
33	Laboratory	Sisters_1	8.8	0.8	86	132	27	28	12	24	Subsurface	3.0	263
34	Laboratory	Sisters_1	6.8	2.8	78	92	22	24	10	18	Subsurface	0.6	271
35	Laboratory	Sisters_1	7	7	90	88	15	33	8	41	Subsurface	2.0	269
36	Laboratory	Sisters_1	7.6	2.3	69	77	23	24	7	48	Surface	3.0	324
37	Laboratory	Sisters_1	13	2	69	62	18	14	10	54	Subsurface	3.1	277
38	Laboratory	Sisters_1	5	3.3	88	43	6	10	20	54	Surface	2.0	300
39	Laboratory	Sisters_1	7.5	4	104	195	15	7	14	74	Subsurface	1.8	246
40	Laboratory	Sisters_1	9.3	2	72	110	14	10	12	41	Surface	11.9	286
41	Laboratory	Sisters_1	3.8	1.3	130	175	10	8	21	63	Surface	2.0	269
42	Laboratory	Sisters_1	8.4	4	77	74	12	7	9	66	Surface	14.3	281
43	Laboratory	Sisters_4	10.5	4.4	65	74	54	49	14	44		Did not smoulder	
44	Laboratory	Sisters_4	10.5	4.4	65	74	23	84	14	44	Surface	8.9	327
45	Laboratory	Sisters_4	6.4	5.1	65	81	77	37	8	63	Surface	11.1	300
46	Laboratory	Sisters_4	6.1	6.1	65	79	41	47	9	26	Surface	2.6	279
47	Laboratory	Sisters_4	6.6	6.4	57	72	35	54	11	31	Surface	13.4	293
48	Laboratory	Sisters_4	8.4	6.4	51	80	98	64	7	35	Surface	2.3	305
49	Laboratory	Sisters_4	9.9	6.3	60	71	68	79	5	18	Surface	4.4	303
50	Laboratory	Sisters_4	8.5	7.6	62	79	88	63	6	26	Surface	1.0	273
51	Laboratory	Sisters_4	8.5	3.3	49	66	59	40	8	47	Surface	3.7	291
52	Laboratory	Sisters_4	7.1	3.5	45	85	64	65	9	36	Surface	1.1	296